Influence of nanoparticle flows on the dynamics of miscible fronts in a Hele-Shaw cell

Karim Ghesmat, Hassan Hassanzadeh, Jalal Abedi, and Zhangxin Chen

Department of Chemical and Petroleum Engineering, University of Calgary, Calgary, Alberta, Canada

Abstract

In this study, we have made an attempt to address how the nanoparticle flows may affect the hydrodynamic instability around a miscible front. In order to explore the role of nanoparticles in such flows, a linear stability analysis was performed to examine the impact of nanoparticle addition for an already unstable miscible displacement. The growth rates of the temporal modes of the instability are determined for different profiles or physical properties of nanoparticles. The results reveal that the diffusion of either the carrier fluids or nanoparticles initially has destabilizing effects, but demonstrates stabilizing effects at longer times, as the cutoff spectrum is initially shifted to larger wavenumbers, but shifted back later. It was found that deposition of nanoparticles into the medium stabilizes the miscible front, such that the maximum growth rates and cutoff wavenumbers increase continuously.

I. Introduction

Application of nanoparticles in porous media and micro channels has recently received great attention [1,2,3]. Nanoparticles can cost-effectively address some of the challenges related to the flow of nanofluids in porous media and micro channels, which range widely in contaminant removal from soil, energy recovery from unconventional resources, and biomedical applications. In the future, new applications may be found for implementing nanoparticles in porous media, such as nano-magnetic imaging for pores illusion or manufacturing functionalized nanoparticles acting at interfaces.

There are usually some important features that determine the capabilities of nanoparticles as an extremely versatile tool. One is their small particle size (1-100 nm). Nanoparticles are also able to form stable suspensions that can last for a long period of time; and, they can be transported into micropores effectively by flow either via injection or gravity. However, there can be difficulties during nanoparticle usage in porous media or microchannels. One involves the mobility of these particles, which represents how far the particles may travel in the micropores and microchannels. Another issue is likely the deposition of the particles to the media, which can highly affect the process[4].

Factors influencing the process also include the particle number density, surface characteristics of the nanoparticles and mineral grains, the pH and ionic strength of the suspending and host fluids, injection rates, the miscibility of the injected and host fluids, and the morphology of the micropore networks in the porous bed. Although the actual relevance of each factor is unknown and still under examination, it is important to mention that the particle position and the forces to which the particles are subjected play key roles in most of these factors, thus showing the need to develop mathematical and numerical models to simulate such flows. A large variety of studies in the field of nanofluids have been conducted to experimentally examine the qualification of nanoparticle applicability in porous media[5,6] ; however, there are still few works that model the hydrodynamics of such flows.

For energy and environment applications, nanoparticles are usually carried by another fluid and delivered at an injection point. This carrier phase can be different from the host phase in micropores and micro channels. The difference between the physical properties of the carrier and the host fluids in micropores and microchannels has already been shown to result in hydrodynamic instability[7]. In fact, the success of nanoparticle implementation in porous media is closely related to this hydrodynamic instability. However, the role of nanoparticles in these types of instabilities is yet unknown.

There are some experimental and numerical models[8,9,10] for the flow of nanoparticles in microchannels or micropores; however, there is still no model available for the flow of nanoparticles involved in hydrodynamic instability. The stability of miscible fronts in porous media has been studied extensively in the literature. However, the effect of the addition of non-reacting nanoparticles, which have recently been applied in various fields, has not been investigated in the past. We have investigated the effect of the addition of reacting nanoparticles on the stability of reactive fronts in porous media. In this work, however, our focus is on the effect of the addition of non-reacting nanoparticles on the hydrodynamic stability of an already unstable miscible front in porous media. To our knowledge, such an analysis has not been presented in the past.

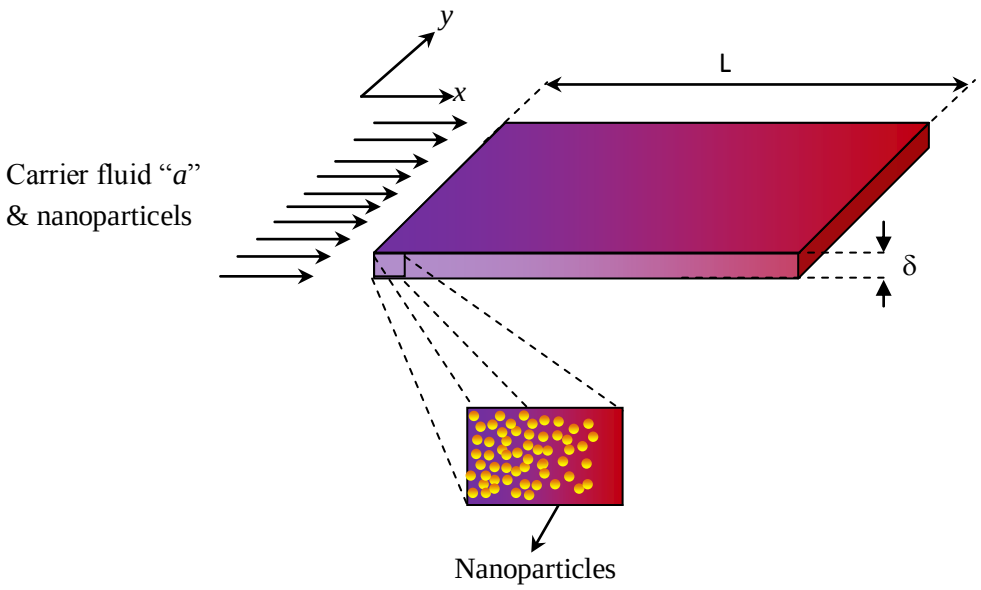

Fig.1. Schematic of nanoparticle flows in a microchannel

II. Theory

A. Flow System Geometry

In the present study, a three-dimensional Hele-Shaw cell is considered, where fluid *a* carries nanoparticles, n_p, and is injected at the left boundary of a microchannel of an infinitesimally small gap. The gap between the upper and lower surfaces, δ, is considered very thin at the micro scale, such that $\delta << L, H$. This allows for the averaging of the fluid properties in the gap direction and simplification of the problem into a two-dimensional one. The length of the domain is assumed as *L*, which is in the order of the macro scale. Fluid *b* is considered to be the host fluid in the microchannel. The fluids are assumed to be Newtonian and incompressible. The viscosity of displacing fluid *a* is less than displaced fluid *b*, such that an ascending viscosity profile is established along the domain. The viscosity increases by increasing the mass fraction of either fluid *b* or the nanoparticles.

B. Governing Equations

Assuming the continuum approach to be valid for a transient laminar incompressible flow in a microchannel[9] , the momentum and species transfer equations have to be solved. To develop a model for such flows, the mass conservation equation is written for fluids *a* and *b* as follows:

$$(a)_t + \mathbf{u}.\nabla a = D_a \nabla^2 a, \tag{1}$$

$$(b)_t + \mathbf{u}.\nabla b = D_b \nabla^2 b, \tag{2}$$

where *a, b,* $\mathbf{u}$ (u,v,w), D_a, and D_b represent the concentrations of fluids *a* and *b*, the velocity vector, and the molecular diffusion coefficients of fluids *a* and *b*, respectively.

The governing equation for the incompressible Newtonian flow in microchannels is:

$$-\nabla p + \nabla.\boldsymbol{\tau} = \partial_t \mathbf{u} + \mathbf{u}.\nabla \mathbf{u} \tag{3}$$

$$\nabla.\mathbf{u} = 0, \tag{4}$$

In the above equations, $\boldsymbol{\tau}$ represents the contribution of the Newtonian fluid to the total stress, and p stands for the local pressure. Because we are dealing with low Reynolds and creepy flows in this work, we may further simplify the Navier-Stokes equation. If the width of the gap is small enough and at the micro scale, the fluid flow can be assumed to be quasi two-dimensional. The equation for this two-dimensional gap-averaged velocity is obtained by applying the following averaging operator to the Navier-Stokes equations:

$$\langle ... \rangle = \frac{1}{2d}\int_{-d}^{+d} dz..., \tag{5}$$

where $d = \delta/2$. After doing some algebra and taking the average over the gap, the final velocity equation for the Hele-Shaw cell is:

$$\nabla p = -\frac{\mu}{\delta^2/12}\mathbf{u}, \tag{6}$$

The governing equation for the concentration distribution of Brownian particles over a surface in the presence of interaction forces is[11,12]:

$$\left(n_p\right)_t + \mathbf{u}.\nabla n_p = \nabla.\left(D_{np}\nabla n_p + m.n_p\nabla\Phi\right), \tag{7}$$

where n_p is the particle concentration, m is the particle mobility, Φ represents the total colloidal interaction energy, and D_{np} is the nanoparticle diffusion coefficient defined by the Stoke-Einstein equation:

$$D_{np} = \frac{k_B T}{6\pi\mu d_{np}} \tag{8}$$

where k_B = 1.38065×10^{-23} m^{2}kg/s^{2}K and is the Boltzman constant, T is temperature, μ is the dynamic viscosity, and d_{np} is the nanoparticle diameter. It is necessary to mention that, to achieve species mixing, the diffusion time in the axial flow should relate to the minimum microchannel length.

Nano and micro scale interactions of the particles at the micropore scale may result in deposition and release of particles to or from the medium[13,14]. The presented relationships for the release or deposition of nanoparticles can be based on a critical velocity or a kinetic form indicating the rate of deposition. In the present study, we use a kinetic formulation for the interaction of nanoparticles, which can be simply shown as a first-order rate of deposition[15,16]:

$$\nabla.\left(m(np)\nabla\Phi\right) = -k_{dep}np \tag{9}$$

where k_{dep} is positive and represents the deposition rate constant. The deposition rate constant, k_{dep}, depends on the molecular interaction and electrostatic forces; and, any change in these forces is reflected in this constant. The initial and boundary conditions for the above equations are:

$$a(x,0) = np(x,0) = 0\,, b(x,0) = b_0 \tag{10}$$

$$a(0,t) = a_0 \;\;,\; b(0,t) = 0 \;\;,\;\; np(0,t) = np_0 \tag{11}$$

$$a(L,t) = np(L,t) = 0\,,\;\; b(L,t) = b_0 \tag{12}$$

In this study, we assume that the initial concentrations of components a and b are equal to a_0 = b_0 and the initial injection velocity is U_0. Viscosity is defined as a function of the concentrations of all components (a, b and np), such that $\mu(a_0,0,0) = \mu_0$ and $\mu(0,\ b_0,0) = \mu_1$ where $\mu_1 > \mu_0$. As shown, the addition of nanoparticles affects the viscosity and, in turn, the hydrodynamics of the flow system. The relationship between viscosity and concentration can be shown with functions used previously by Ghesmat & Azaiez[17]. The viscosity of the solution can be even affected by the addition of nanoparticles when the particle concentration is enough large, as described by:

$$\mu = \bar{\mu}\, e^{\left(R_a c_a + R_b c_b + R_c np\right)/\, a^*_0} \tag{13}$$

where $\bar{\mu}$ is a constant, and R_a, R_b and R_{np} are log mobility ratios defined at concentrations a_0, b_0 and np_0, respectively:

$$R_a = \ln\left(\frac{\mu_0}{\bar{\mu}}\right) \qquad R_b = \ln\left(\frac{\mu_1}{\bar{\mu}}\right) \qquad R_{np} = \ln\left(\frac{\mu_{np_0}}{\bar{\mu}}\right) \tag{14}$$

The equations are made dimensionless using a diffusive scaling method, and the coordinate is changed from a fixed one to a reference frame moving at a constant velocity. Thus, we scale all lengths by the diffusion length, D_a/U_0, time by the diffusive time, D_a/U_0^2, viscosity by $\bar{\mu}$, concentration by c_{a0}, and velocity by U_0. The coordinate is also changed to a moving reference at velocity U_0:

$$\hat{\mathbf{u}} = \mathbf{u} - U_0\mathbf{i} \tag{15}$$

The domain length in the flow direction is also shown by the Peclet number, $Pe = U_0L/Da$, using the above scaling criteria. By dropping all hats, the equations of motions are then converted into:

$$\mathbf{u} + \mathbf{i} = -\frac{\delta}{12\mu}\nabla p \tag{16}$$

$$\nabla.\mathbf{u} = 0 \tag{17}$$

Using the same procedure, the mass conservation equations are changed into:

$$\frac{\partial a}{\partial t} + \mathbf{u}.\nabla a = \nabla^2 a \tag{18}$$

$$\frac{\partial b}{\partial t} + \mathbf{u}.\nabla b = D_b^*\nabla^2 b \tag{19}$$

$$\frac{\partial np}{\partial t} + \mathbf{u}.\nabla np = D_{np}^*\nabla^2 np - Da_{dep}.np \tag{20}$$

In the moving reference frame, the concentrations of species *a* and *b* and the nanoparticles are set to 1, 0 and n_{p0}, respectively, at the injection point and 0, 1, 0, respectively, at the end of the domain. As the dilute nanoparticle is usually applicable, n_{p0} is set to either 0.02 or 0.05 in the following discussion, while the logarithmic viscosity ratios are set as -3, 0, 2 for fluids *a* and *b* and the nanoparticles. The base state time, t_0, is also fixed at 5 in this study, unless its sensitivity is being

examined. Deposition Damkohler (Da_{dep}) and Peclet (Pe) numbers are important dimensionless groups representing the rates of deposition and injection and are constant as Da_{dep} = 0.02 or 0.4 and Pe = 1500, respectively. The dimensionless initial and boundary conditions for the above equations are:

$$a(x,0) = np(x,0) = 0,\ b(x,0) = b_0 \tag{21}$$

$$a(-t,t) = a_0\ ,\ b(-t,t) = 0\ ,\ \ np(-t,t) = np_0 \tag{22}$$

$$a(Pe-t,t) = np(Pe-t,t) = 0,\ \ b(Pe-t,t) = b_0 \tag{23}$$

To examine how the addition of nanoparticles into the flow system and around the concentration boundary layer may change the hydrodynamical stability of the flow system, a linear stability analysis is employed. To conduct the linear stability analysis for the above system, the concentration boundary layer is perturbed at the base state, such that:

$$\Re(x,y,t) = \overline{\Re}(x,t) + \Re'(x,y,t), \tag{24}$$

where $\Re$ accounts for **u**, a, b, p and n_p, and $\overline{\Re}$ represents the base state. The prime term stands for perturbations at the base state frozen at time t_0 as well.

Equation 24 is substituted in Equations 16 to 23, where two sets of equations are obtained for base states and perturbations. The analytical solutions can be sought for fluids a and b and nanoparticles' base states using the separation of variables method. The analytical solutions used here as the base states are all in the form of a Fourier series. We present the analytical solution for the nanoparticle base state (Equation 20), which is a general form. One may set Da_{dep} equal to zero and change np to a and b to find the analytical solution form in a and b base states. The solution for the nanoparticle base state can be obtained using the separation of variable method, as given by Kreyszig[18]:

$$np(x,t)=\frac{np_0}{e^{-2\sqrt{\frac{Da_{dep}}{D_P^*}}(Pe-t)}e^{-\sqrt{\frac{Da_{dep}}{D_P^*}}t}-e^{\sqrt{\frac{Da_{dep}}{D_P^*}}t}}\left(e^{-\sqrt{\frac{Da_{dep}}{D_P^*}}x}-e^{-2\sqrt{\frac{Da_{dep}}{D_P^*}}(Pe-t)}e^{\sqrt{\frac{Da_{dep}}{D_P^*}}x}\right)+$$

$$\sum_{n=1}^{\infty}A_n\left(\sin\left(\frac{n\pi}{Pe}x\right)+\frac{\sin\left(\frac{n\pi}{Pe}t\right)}{\cos\left(\frac{n\pi}{Pe}t\right)}\cos\left(\frac{n\pi}{Pe}x\right)\right)e^{-\left(\frac{D_P^*n^2\pi^2}{Pe^2}+Da_{dep}\right)t} \tag{25}$$

where A_n is given by:

$$A_n=-\frac{2n\pi cnp_0}{Pe^2\left(1-e^{-2\sqrt{\frac{Da_{dep}}{D_P^*}}Pe}\right)\left(\frac{Da_{dep}}{D_P^*}+\frac{n^2\pi^2}{Pe^2}\right)}\left[\left(e^{-2\sqrt{\frac{Da_{dep}}{D_P^*}}Pe}-1\right)-2(-1)^n e^{-\sqrt{\frac{Da_{dep}}{D_P^*}}Pe}\right] \tag{26}$$

The perturbation and base state terms is substituted in equations 16-20 for velocities and concentration of fluids *a* and *b* and nanoparticle. The model equations describing the system are expressed in terms of the base state plus perturbations, and are linearized by dropping second- and higher order terms. If the second-order and higher-order terms are neglected, then a linear equation for the perturbation $\Re'(x,y,t)$ is obtained. Using normal mode decomposition, the perturbation can be written in terms of its Fourier components. Using the Fourier decomposition mode, the perturbation term is written as $\Re'(x,y,t)=\tilde{\Re}(z)e^{i\,k+y\omega t}$, and the solution is sought in terms of normal modes. Parameters *k* and ω stand for the perturbations' wavenumber and growth rate, respectively. The resulting linearized forms of Equations 1-5 are:

$$(\tilde{a})_{xx}-(k^2+\omega)\tilde{a}=(a_0)_x, \tag{27}$$

$$(\tilde{b})_{xx}-(k^2+\omega)\tilde{b}=\chi(b_0)_x, \tag{28}$$

$$D_P^*\left(\tilde{n}_p\right)_{xx} - \left(k^2 D_P^* + Da_{dep} + \omega\right)\tilde{n}_p = \chi\left(n_{p0}\right)_x, \tag{29}$$

$$\left(\chi\right)_{xx} - \left[R_a\left(a_0\right)_x + R_b\left(b_0\right)_x + R_{np}\left(n_{p0}\right)_x\right]\chi_x - k^2\chi = R_a k^2\tilde{a} + R_b k^2\tilde{b} + R_{np}k^2\tilde{n}_p, \tag{30}$$

where $\tilde{a},\tilde{b},\tilde{n}_p$ and χ are the concentrations of fluids *a* and *b* and the nanoparticles and the velocity eigenfunctions, respectively. The variables with zero subscripts represent the base state functions, while the subscript *x* shows the corresponding derivative. The problem is solved using a quasi-steady-state assumption (QSSA), where t_0 represents the related frozen time. The boundary conditions that are required to solve the equations are:

$$\tilde{a} = \tilde{b} = \tilde{n}_p = \chi = 0 \qquad \text{as} \qquad x = -t \text{ and } x = Pe-t. \tag{31}$$

As the coefficients of the above equations are independent of the *y*-direction, we may use the Fourier decomposition modes in that direction. We also implement the QSSA used by Tan and Homsy (1986). In the above formulation, the base state is a function of both time (*t*) and space (*x*). To use the standard linear stability analysis approach, the time dependence of the base state is eliminated using the QSSA. Using this approximation, one assumes that the growth of perturbations in time is much faster than that of the base state, allowing for the treatment of the base state as if they were steady by freezing them at one time.

The above set of equations (Equations 27-31) is an eigenvalue problem, where the growth rate corresponding to each wavenumber is found numerically using a logarithmic finite difference scheme. The spatial derivatives are approximated using second-order central difference formula. A non-uniform geometric mesh is used which is very fine around the interface where the concentration gradients are large, and spacing increases geometrically with the distance from the origin. All eigenfunctions are discretized using this technique, and the computation domain is chosen wide enough to capture all the eigen-solutions. We used a mesh number of 300 for the discretized problem. One may note that the

above eigenvalue problem reaches an analytical solution ($\omega = -k^2$) at small times ($t_0 = 0$), when the concentration of nanoparticles is zero. The numerical code is validated by checking this special case. The code becomes more validated by solving the eigenvalue problems for different number of meshes. The results have been tested for mesh numbers of 100, 200 and 300. Different logarithmitic space values have been also checked for the convergence of the numerical. In addition, the concentration eigenfunctions were plotted to assure that the eigenfunctions are converged and decay along the domain and in the flow direction. It should be mentioned that the step function solution ($t_0 = 0$) is different from the classic work of Tan and Homsy (1986), where they had the miscible interface at the middle of the geometry and found that the step function always results in the most unstable growth rate. However, as we are dealing with an unperturbed boundary condition at the inlet, the flow system turns out to be totally stable. Their results may be recoverable, if we deal with a miscible interface at the middle of the geometry instead. In fact, in the classic works of viscous fingering, the introduced perturbations are placed in both fluids *a* and *b* on the left- and right-hand sides of front. Using a jump condition, this could result in an analytical solution and the solution gives the most unstable mode at $t_0 = 0$. In our study, however, the step function profile results in a system in which perturbations are placed in only fluid *b*, right after the injection point. In this case, fluid *b* is only in contact with fluid *a* and nanoparticle *np* at the boundary. In this scenario, the jump condition cannot be valid, as the boundary is assumed to be unperturbed. In fact, this may lead to find the most unstable modes at times larger than zero. Changing the parameters in the flow system, can definitely affect the turnaround time to even less than 50 and close to zero. In what follows, the impact of different nanoparticle physical properties and profiles on the hydrodynamic stability of the miscible front is discussed.

III. Results and Discussions

A. Effect of Diffusion Time

We first examine the effect of diffusion time or front sharpness on the hydrodynamic stability of the miscible front in the presence of nanoparticles. Fig. 2 shows a dispersion curve for different t_0. The figure reveals that the range of unstable spectrum wavenumbers is either negative or at small values when the front is very sharp. However, the concentration boundary layer becomes completely unstable as time passes. $t_0 = 50$ seems a turning point, as diffusion plays a destabilizing role for times shorter than 50, while it has a stabilizing effect for times longer than 50. Turnaround time ($t_0 = 50$) is a function of system parameters and could be shifted towards the smaller values choosing other values for t0 and aspect ratios.

Diffusion and convection are the two mechanisms that compete here to drive the instability. It has been previously shown[17] that, when a less viscous fluid displaces a high viscous one, the miscible front is destabilized due to viscous forces. Here, diffusion acts to increase the size of diffusive concentration boundary layer, which then becomes unstable due to viscous forces. In fact, diffusion initially helps as the viscosity difference, which is the main source of instability in this problem, gets established. This can be the reason why cutoff wavenumbers initially move towards the larger numbers, and diffusion plays a destabilizing role. However, as the diffusion time increases, the concentration field and, consequently, the viscosity profile become relatively more homogeneous, and the flow system turns more stable. Indeed, increasing the size of the diffusive concentration boundary layer due to diffusion results in a weakening in the viscous forces and, thus, a more stabilized miscible front.

B. Effect of Nanoparticle Logarithmic Viscosity Ratio

With the addition of nanoparticles, the main change in the physical property that drives the instability is viscosity. Even the addition of a small amount of nanoparticles can significantly vary the viscosity. The impact can be an increased or reduced viscosity[19]; however, in most cases, the viscosity increases with the addition of nanoparticles.

To have a better understanding of the viscosity influence by nanoparticles on the instability trend of a front, the maximum growth rate contours for different viscosity ratios are shown in Fig 3. Figs. 3(a) and 3(b) show the dispersion curves for different nanoparticle logarithmic viscosity ratios, R_{np}, at two different concentrations (np_0 = 0.05 and np_0 = 0.02), while the rate of nanoparticle deposition is constant at 0.02 (which a small rate). The logarithmic viscosity ratios for fluids *a* and *b*, R_a and R_b, are assumed to remain constant. As indicated, the miscible front becomes less unstable as the logarithmic viscosity ratios increases. An increment in the nanoparticle logarithmic viscosity ratio, R_{np}, results in more viscous displacing fluid; consequently, the viscosity difference between the displacing and displaced fluids is decreased with the addition of nanoparticles, as the nanoparticle logarithmic viscosity ratio increases. This, in turn, results in less pronounced viscous forces when R_{np} is large, such that the flow system becomes less unstable.

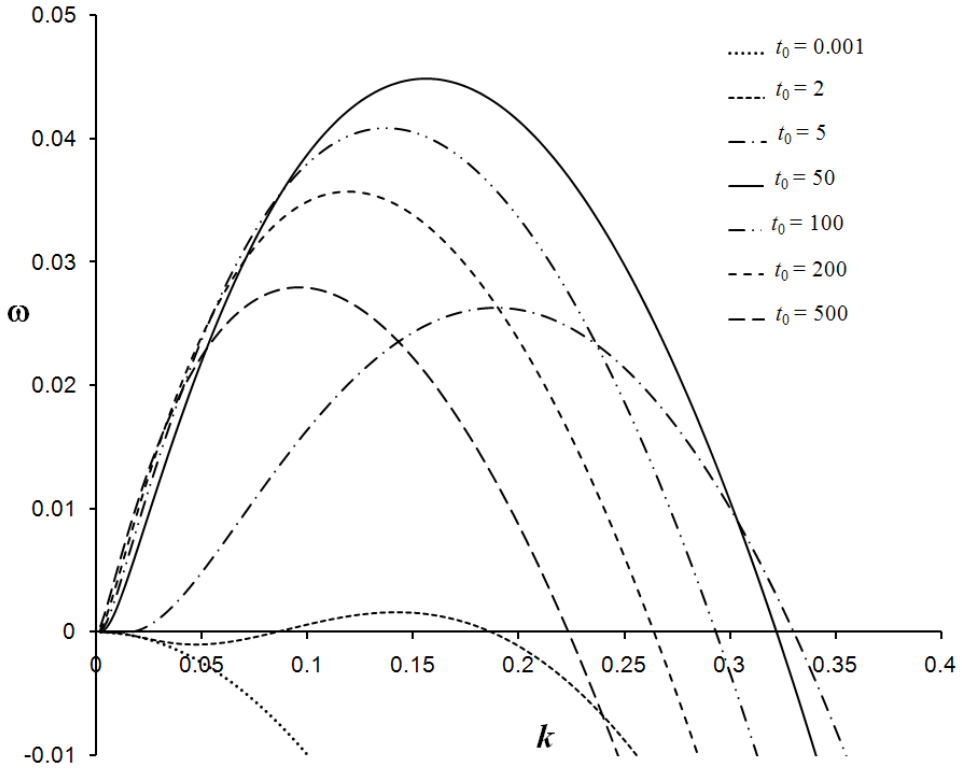

Fig. 2. Variation of the growth rate versus wavenumber at different t_0, Pe = 1500, D_{np} = 1 and Da_{dep} = 0.02.

A comparison between Figs. 3(a) and 3(b) reveals that the flow systems are more stable for a system with a higher concentration of nanoparticles. Finally, Fig. 3(c) shows the variation in the maximum growth rate versus the wavenumbers for a higher rate of deposition. In this scenario, the trend of dispersion curves is closer to the flow system with a lower concentration. A more comprehensive examination of nanoparticle concentration and deposition effects is discussed later. In general, when the nanoparticle logarithmic viscosity ratio is larger, the increasing effect of viscosity is more pronounced along the domain, and a more uniform viscosity profile is established from downstream to upstream. Thus, one may expect a more stable front as the nanoparticle logarithmic viscosity ratio increases.

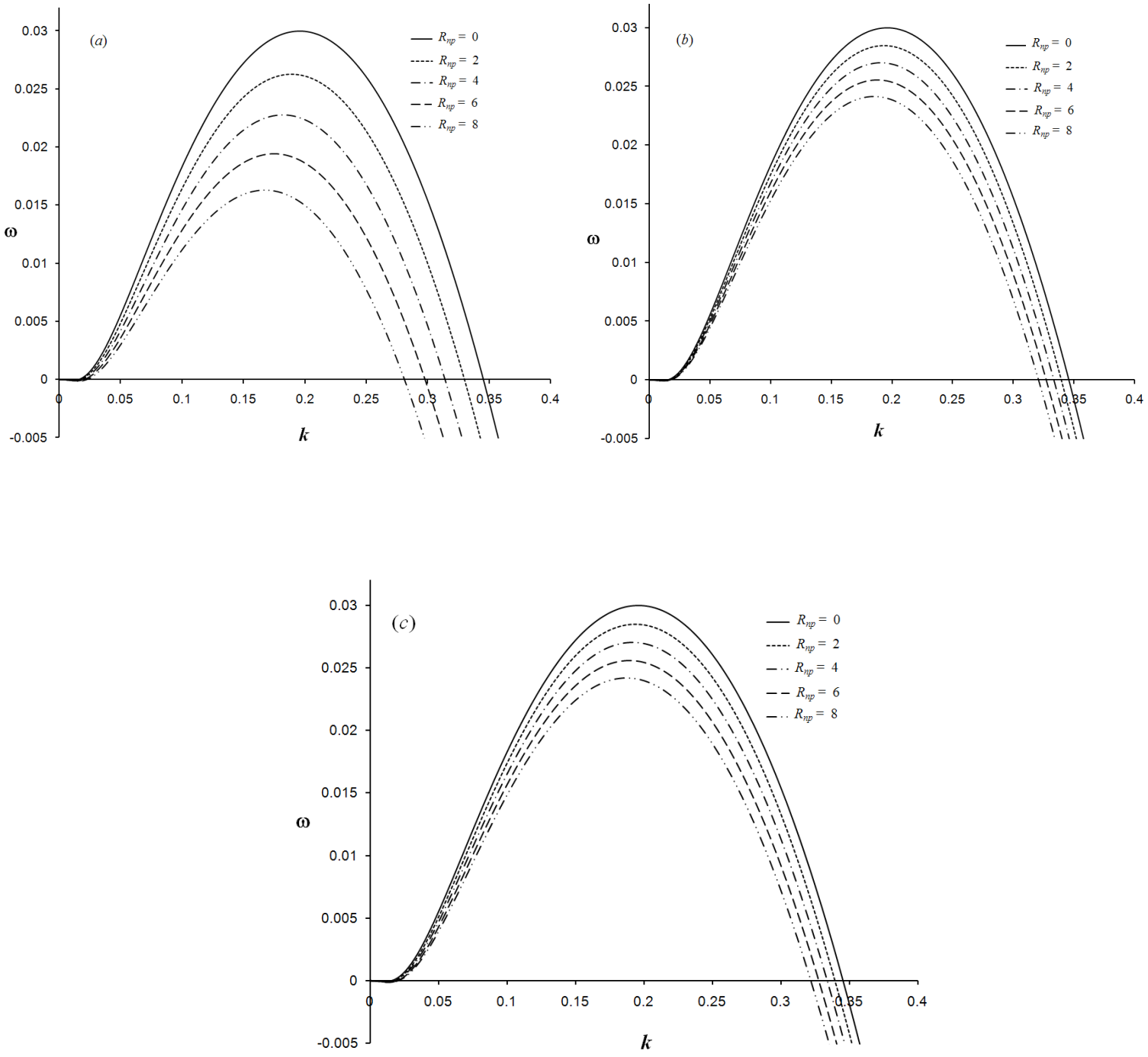

Fig. 3. Variation of the growth rate versus wavenumber at different nanoparticle logarithmic viscosity ratios at Pe = 1500, D_{np} = 1: a) np_0 = 0.05 and Da_{dep} = 0.02; b) np_0 = 0.02 and Da_{dep} = 0.02; c) np_0 = 0.05 and Da_{dep} = 0.4.

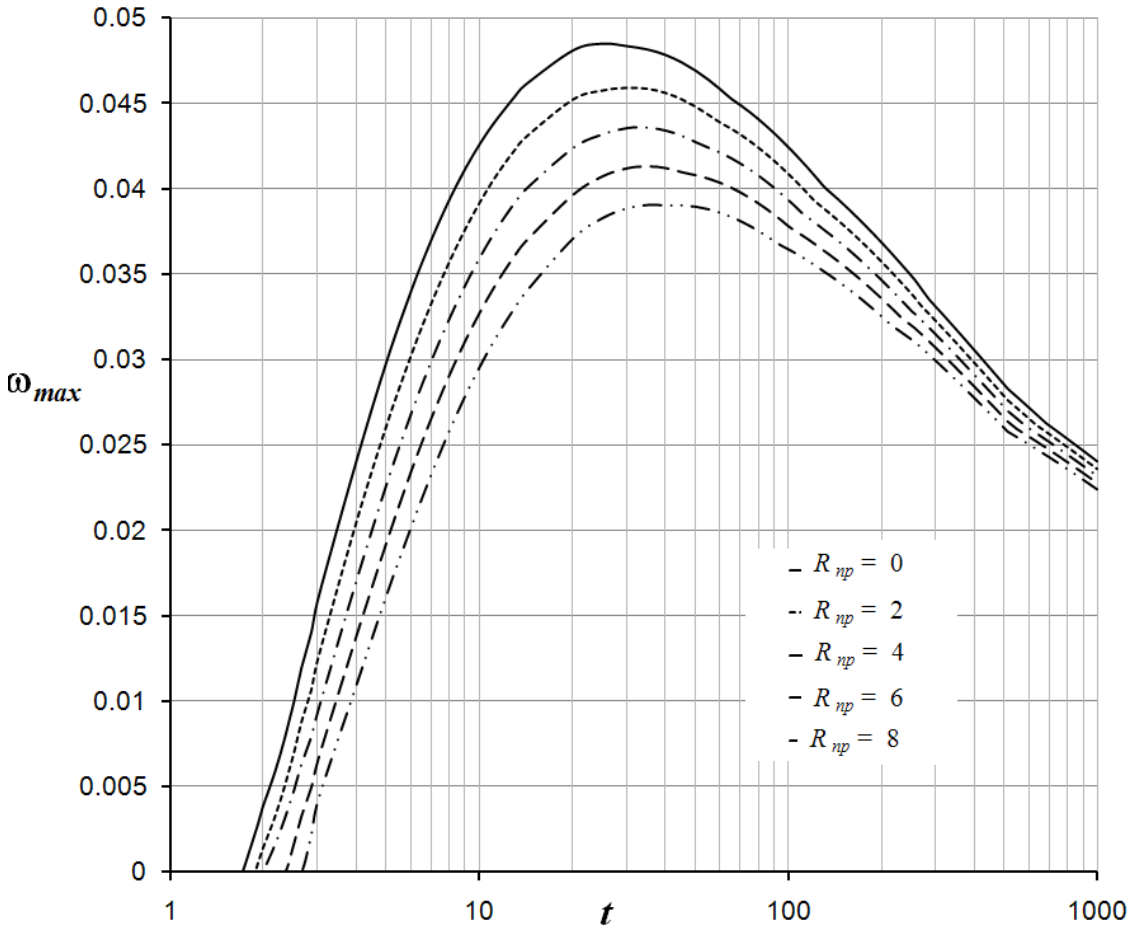

Fig. 4. Variation of the maximum growth rate versus time at nanoparticle logarithmic viscosity ratios, R_{np}: Pe = 1500, D_{np} = 1 and Da_{dep} = 0.02.

In order to analyze further the impact of nanoparticle logarithmic viscosity ratio on the stability of the flow system, the variation of the maximum growth rate at different times was plotted, as illustrated in Fig. 4. The figure shows that the flow system is initially stable at small times. However, the flow system becomes unstable as time increases. In fact, the thickness of concentration boundary layer increases by diffusion, as discussed previously; and, the difference in the viscous forces becomes more significant. The established viscosity profiles become more uniform as the diffusion time

increases, and the flow system becomes less unstable at long times. A time of 50 seems to be critical for the destabilizing and stabilizing role of diffusion, independent of nanoparticle logarithmic viscosity ratios, R_{np}. One may find that the maximum growth rates merge into a single value at a very long diffusion time.

C. Effect of Nanoparticle Concentration

Nanoparticles are usually used in low concentrations; however, the concentration may be high around the front due to reasons such as accumulation or aggregation. Indeed, Fig. 5 shows how the concentration of nanoparticles may affect the hydrodynamic stability of the front. The flow system becomes more stable with a decrease in both the cutoff wavenumber and the maximum growth rate, as the concentration of nanoparticles behind the injection point increases. As before, we may argue that the viscous forces are stronger when the nanoparticle concentration is low in the medium. In fact, the addition of nanoparticles has an increasing effect on the viscosity of the fluid, while all of the concentration profiles remain unchanged. Consequently, the viscosity difference between the displacing and displaced fluids decreases as the inlet concentration of nanoparticles increases. This, in turn, can result in a more stable flow system.

A further investigation examines how the concentration of nanoparticles and the nanoparticle logarithmic viscosity ratio may influence the hydrodynamics of the flow system. Figs. 6(a) and 6(b) represent the variation of contours of the maximum growth at different nanoparticle viscosity ratios and concentrations at two different rates of nanoparticle deposition. As seen, the instability is always at its highest when either the nanoparticle concentration or R_{np} is small. Fig. 6 also reveals that the unstable zone shrinks when the rate of nanoparticle deposition increases.

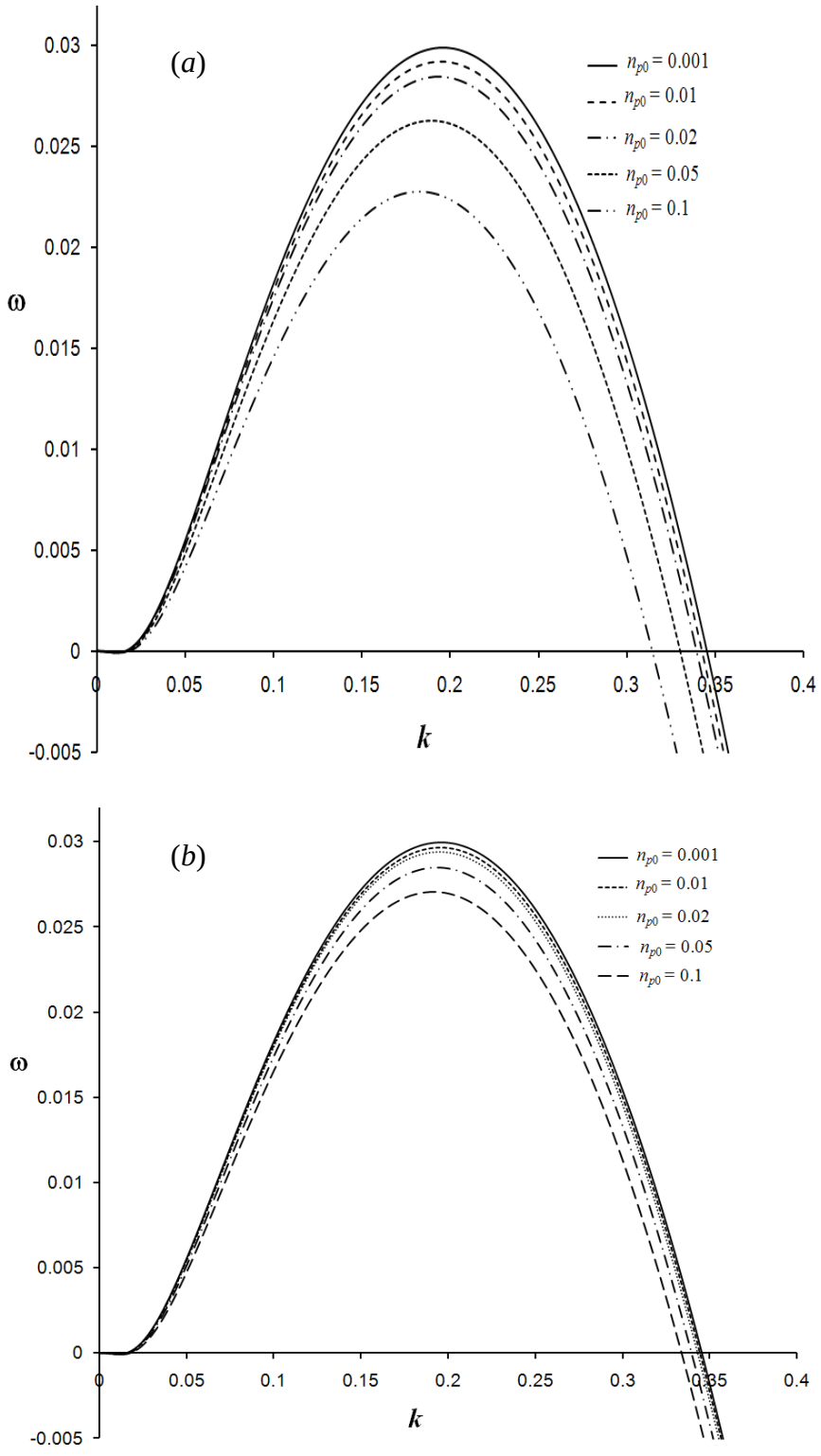

Fig. 5. Variation of the growth rate versus wavenumber at different nanoparticle concentrations at Pe = 1500, D_{np} = 1: a) Da_{dep} = 0.02; b) Da_{dep} = 0.4.

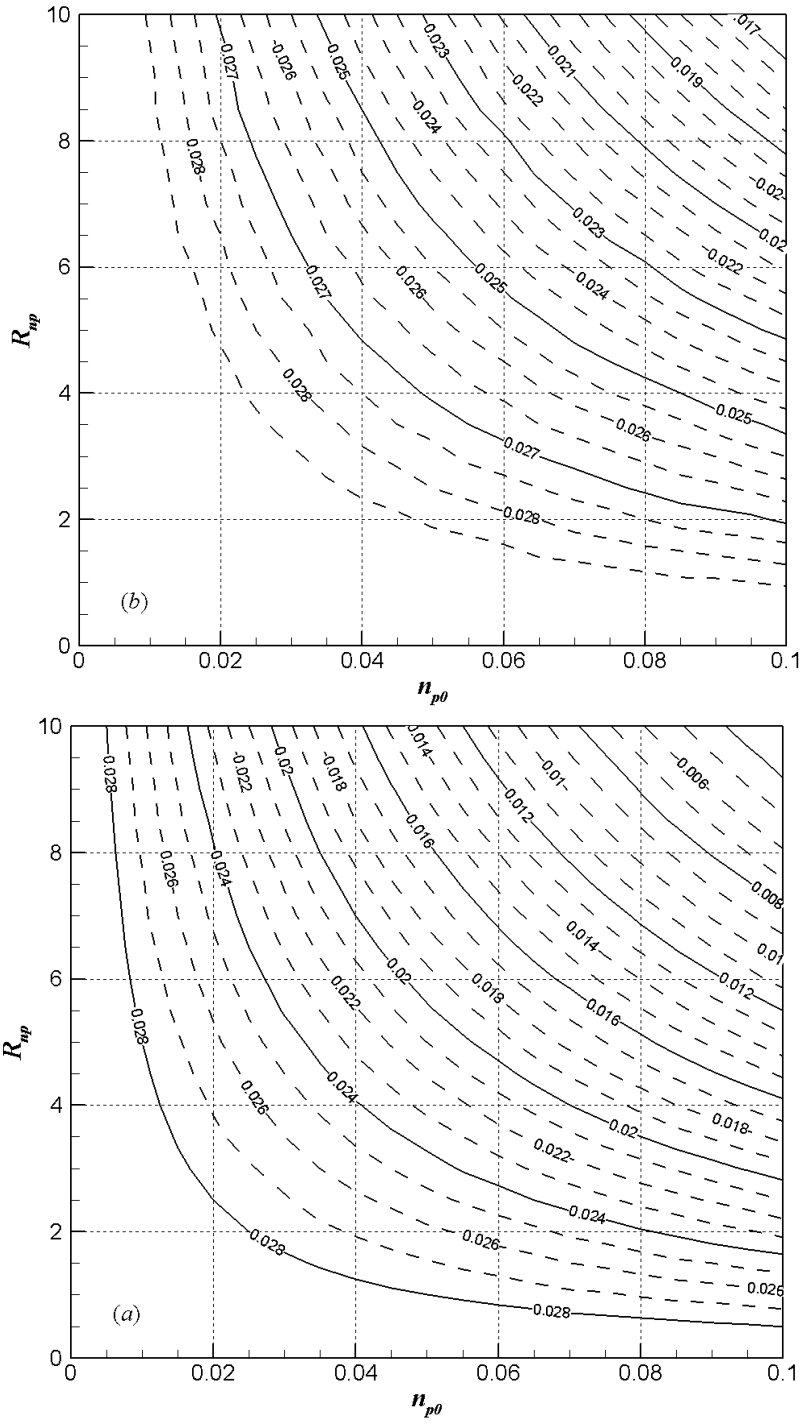

Fig. 6. Contours of the maximum growth rates for different nanoparticle logarithmic viscosity ratios and concentrations at Pe = 1500, D_{np} = 1: a) Da_{dep} = 0.02; b) Da_{dep} = 0.4.

As shown before, the diffusion time initially has a destabilizing effect on the flow system and then a stabilizing one; and, a critical time of approximately 50 was found. To examine if this trend and the critical time are affected by the nanoparticle concentration, a plot of the maximum growth rate versus time is shown in Fig. 7. This figure indicates that the same trend is observed here for different nanoparticle concentrations and the critical time remains around the same number with a slight change for different nanoparticle concentrations.

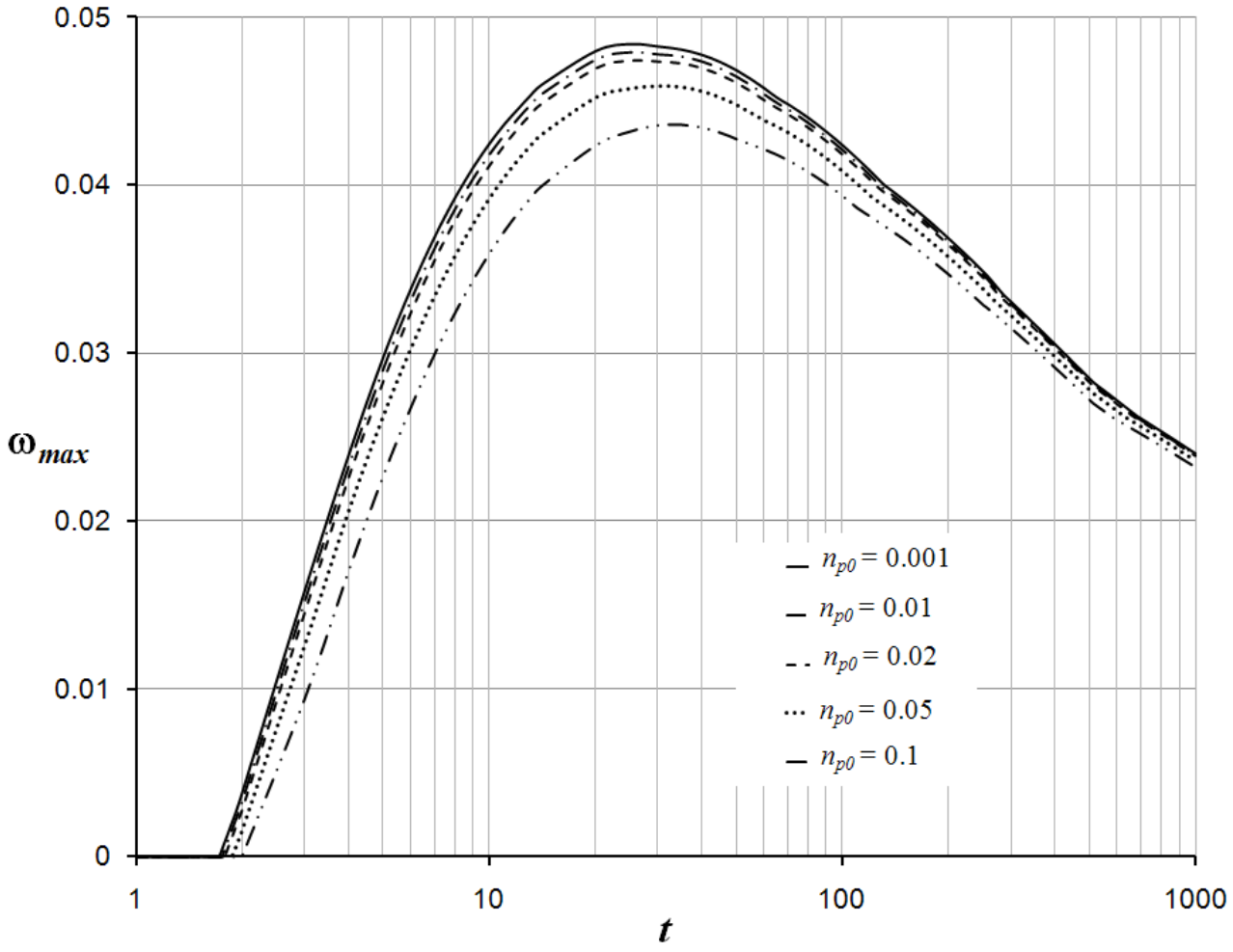

Fig. 7. Variation of the maximum growth rate versus time for different nanoparticle concentrations, $R_{np} = 2$, $Pe = 1500$, $D_{np} = 1$ and $Da_{dep} = 0.02$.

D. Effect of Nanoparticle Rate of Deposition

As previously mentioned, nanoparticles may aggregate and deposit into the medium; therefore, the Brownian motion of the particles and the van der Waals and repulsive forces for the nano scale particles are important. The significance of the nanoparticle deposition, even for a small amount of particle number density, in the microchannels is indicated in Fig. 8, where the stability trend moves toward the larger spectrum of wavenumbers when the rate of deposition increases. The stability trends are the same at both concentrations where the flow system becomes more stable as the deposition rate decreases. The reason for this behavior is clearly hidden in the change of viscosity contrast as the nanoparticles are deposited in the system. In fact, when the nanoparticles are removed from flow system by deposition, the viscosity contrast between two phases is larger. The larger viscosity difference will result in a more unstable miscible front.

Fig. 8 clearly shows that, when the nanoparticle concentration is small, the effect of deposition rate may be negligible. This is also the case when the rate of nanoparticle deposition is adequately large, such that there is a small amount of nanoparticles remaining in the system. In this scenario, the stability curves merge into a single curve.

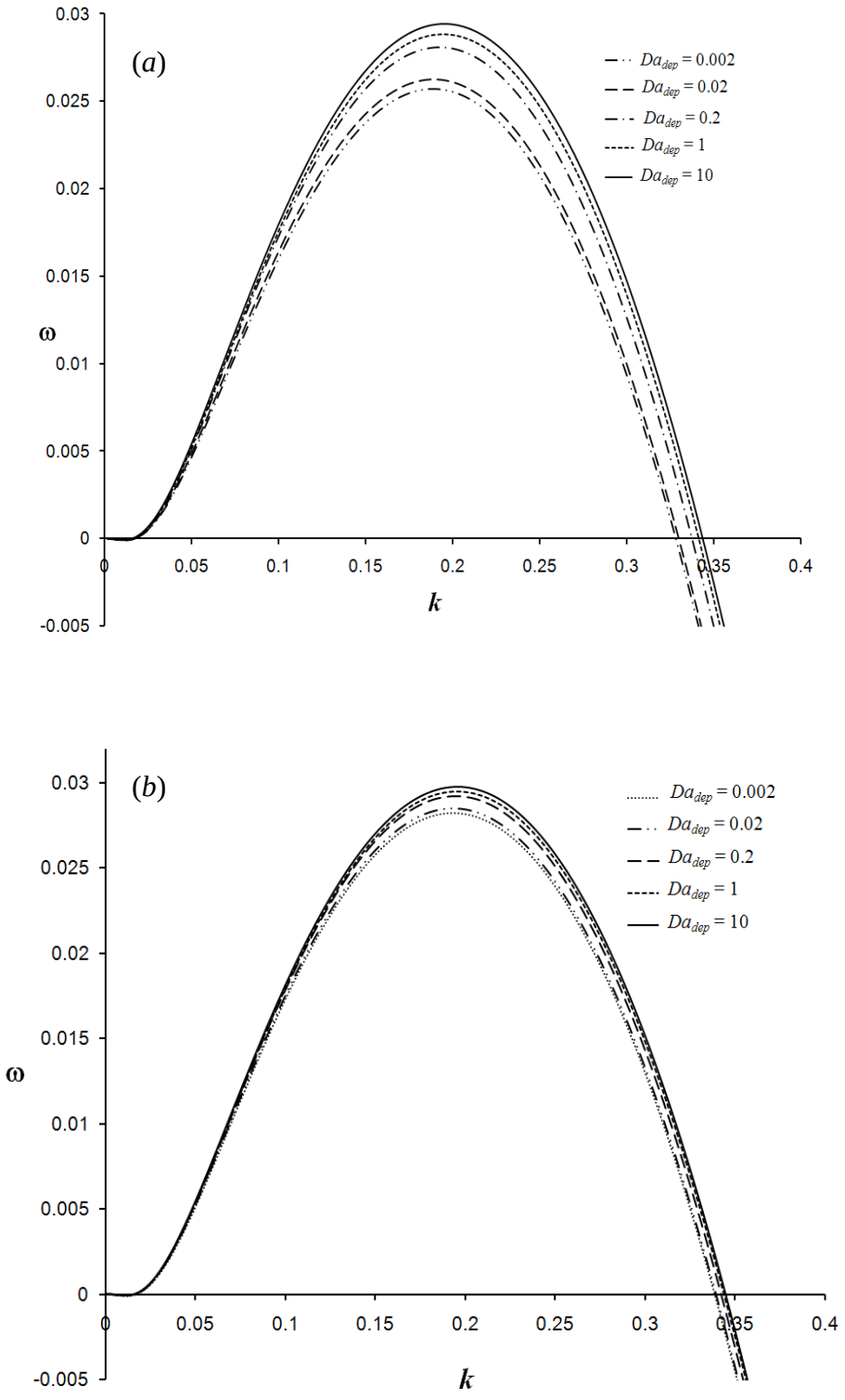

Fig. 8. Variation of the growth rate versus the wavenumber at different nanoparticle rates of deposition at Pe = 1500, D_{np} = 1: a) np_0 = 0.05; b) np_0 = 0.02.

E. Effect of Nanoparticle Diffusion Coefficient

The other physical property of nanoparticles that has a significant role in the applicability of nanoparticles in micropores and micro channels is the diffusion coefficient. The diffusion coefficient's order of magnitude needs to be the same as that of the carrier fluid; however, it may vary depending on the type of particles. As shown by Einstein (1906), the particle size and diffusion coefficient are inversely proportional, such that any variation of the instability trend with the diffusion coefficient may also be considered as an effect of the nanoparticle size.

Figs. 9(a) and 9(b) depict the impact of the nanoparticle diffusion coefficient on the stability of front at two different nanoparticle concentrations. In these scenarios, as the nanoparticle diffusion coefficient increases, the cutoff wavenumbers initially shift to the larger values, whereas the maximum growth rates smoothly increase. While the maximum growth rate begins to shift back to the smaller values, the cutoff wavenumbers decrease when the nanoparticle diffusion coefficient goes over one.

Our physical arguments explaining the stabilizing and destabilizing effects of diffusion may again be implied here. Basically, the nanoparticles can move further as the diffusion coefficient increases, resulting in a more diffusive base state. Again, the nanoparticle may diffuse into the displaced fluid *b* and, in turn, increase the viscosity ratios between fluids *a* and *b*, which drives the instability. In fact, when the diffusion increases the viscosity difference, it would have a destabilizing effect on the miscible front; whereas, it would have a stabilizing effect when reducing the viscosity difference between fluids *a* and *b*. Indeed, this can again be attributed to the destabilizing effect of diffusion around the time of analysis, when the nanoparticle base state becomes more diffusive as the nanoparticle diffusion coefficient, D_{np}, increases.

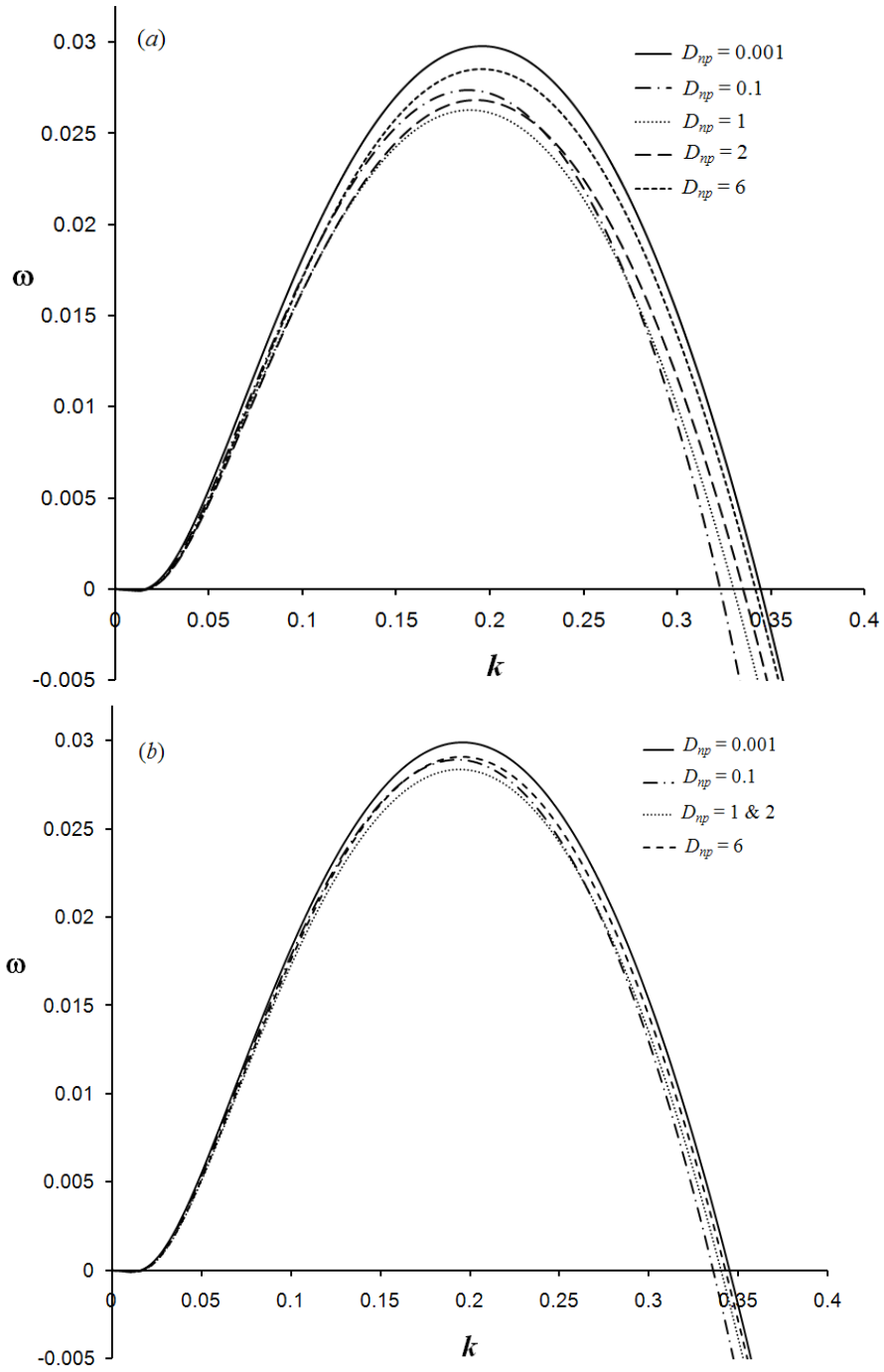

Fig. 9. Variation of the growth rate versus the wavenumber at different nanoparticle diffusion coefficients at Pe = 1500, D_{np} = 1: a) np_0 = 0.05; b) np_0 = 0.02.

IV. Conclusion

In this paper, we have presented the hydrodynamic stability analysis of nanoparticle flows for a flow system in which the viscosity profile is descending along the domain in a horizontal geometry. A thorough examination of the flow system has revealed that the stability of a miscible front is affected by the addition of a small amount of nanoparticles to the displacing fluid. The results also show that increasing of nanoparticle concentration or decreasing of deposition rate has a stabilizing effect for the time of analysis; whereas, the nanoparticle diffusion coefficient can have either a stabilizing effect or a destabilizing. The larger viscosity ratio for nanoparticles has also been found to have a stabilizing impact on the front.

Acknowledgment

The financial support of the Alberta Ingenuity Centre for In Situ Energy (AICISE) is acknowledged.

References

[1] A. J. Pelly, N. Tuefenkji "Effect of particle size and natural organic matter on the migration of nano and microscale latex particles in saturated porous media" *J. Colloid Interface Sci*. **321**, 74-83 (2008).

[2] R. Doshi, W. Braida, C. Christodoulatos, M. Wazne, , G. O'Connor "Nano-Aluminium: Transport through sand columns and environmental effects on planets and soil community". *Environ. Res*. **106**, 296-393 (2008).

[3] S. R. Kanel, D. Nepal, B. Manning, H. Choi "Transport of surface-modified iron nanoparticles in porous media and application to arsenic (III) remediation" *J. Nanopart. Res*. **9**, 725-735 (2007).

[4] X. Liu, M. Wazne, C. Chriostodoulatos, K. L. Jasinkiewicz "Aggregation and deposition behavior of boron nanoparticles in porous media" *J. Colloid Interface Sci*. **330** 90-96 (2009).

[5] T. Phenrat, N. Saleh, K. Sirk, R. D. Tilton, G. Lowry "Aggregation and sedimentation of aqueous nanooscale Zerovalent iron dispersion" *Environ. Sci. Tech* **41**, 284-290 (2007).

[6] R. Prezekop, L. Gradon "Deposition and filtration of nanoparticles in the composite of nano- and microsized fibers" *Aerosol. Sci. Tech.* **42** 483-493 (2008).

[7] C. T. Tan, G. M. Homsy "Stability of miscible displacement in porous media-rectilinear Flow", *Phys. Fluids*. **29**, 3549 (1986).

[8] Y. J. Feng, B.M. Yu, "Thermal conductivity of nanofluids and size distribution of nanoparticles by Monte Carlo simulations" *J. Nanopart. Res.* **8**, 1319-1328 (2008).

[9] J. Li, C. Kleinstreuer, "Microfluidics analysis of nanoparticle mixing in a microchannel system" Microfluid Nanofluid. **6**, 661-668 (2009).

[10] A. V. Kuznetsov, D. A. Nield, "Thermal Instability in a Porous Medium Layer Saturated by a Nanofluid: Brinkman Model" *Transp. Porous. Med*. 81, 409-422 (2010).

[11] C. Tien "Granular Filtration of aerosols and hydrosols" Butterworths publishers: Stoneham, MA. (1989).

[12] L. A. Spielman, S. K. Friedlander "Role of the electrical double layer in particle deposition by convective diffusion" *J. Colloid. Interface. Sci*. **46**, 22 (1974).

[13] E. Ruckenstien, D. Prieve "Adsorption and desorption of particle and their chromatographic separation", *AIChE J*. **22**, 276 (1976).

[14] M. M. Sharma, Y. Yortsos "Transport of particulate suspensions in porous media: model formulation", *AIChE J*., **33**, 1636-1643 (1987).

[15] Y. Chu, Y. Jin, M. V. Yates "Virus transport through saturated sand columns as affected by different Buffer solutions" *J. Environ. Quality*. **29**, 1103-1110 (2000).

[16] Y. Jin, M. V. Yates, S. Thompson, W. A. Jury "Sorption of viruses during flow through saturated sand columns" *Environ. Sci. Tech.* **31**, 548-555 (1997).

[17] K. Ghesmat, J. Azaiez "Viscous fingering instability in porous media: Effect of anisotropic velocity dependent dispersion tensor" *Transp. Porous. Med*. **73**, 297-318 (2008).

[18] E. Kreyszig Advanced engineering mathematics (2006).

[19] M. Mackay, T. Dao, A. Tuteja, D. Ho, B. Horn, H. Kim, C. Hawker "Nano-scale effects leading non-Einstein-like decrease in viscosity", *Nature Materials*. **2**, 762 (2003).

[20] A. Einstein "Eine neue bestimmung der molekuldimensionen" *Ann. Phys.* **29**, 289-306 (1906).